Interchannel Antenna Pattern Correction for Azimuth Digital Beamforming in Airborne SAR

Juan Pablo Navarro Castillo, Rolf Scheiber, Marc Jäger, and Alberto Moreira, *Fellow, IEEE,*

***Abstract*—High-Resolution Wide Swath (HRWS) Synthetic Aperture Radar (SAR) systems are normally designed to have identical antenna patterns in each receive channel. Nevertheless, due to different factors, this condition might not be satisfied, resulting in a multichannel radar system with different antenna patterns. This paper studies the impact of these relative antenna differences on the performance of a state-of-the-art azimuth motion-adaptive image reconstruction for a real airborne SAR sensor with multiple azimuth channels on receive. The performance of the reconstruction algorithm is evaluated both when these relative differences are neglected and when they are accounted for in the multichannel reconstruction process. Additionally, the range dependency of the antenna pattern as a function of wavenumber and the use of range block processing to minimize the impact of this dependency are analyzed. The results confirm the relevance of including these additional steps in the reconstruction, extending the understanding of SAR systems using digital beamforming (DBF) in azimuth.**

***Index Terms*—digital beamforming, azimuth SAR image reconstruction, airborne SAR, antenna pattern, range block processing**

I. Introduction

DBF SAR is a well-known solution to simultaneously achieve a high image resolution and to cover a wide swath [1]. HRWS spaceborne systems are typically composed of a transmitting antenna and several receiving apertures arranged along the flight direction and in elevation, forming a 2D antenna array. The echoes received in each aperture are independently digitalized and post-processed to obtain a SAR image. HRWS systems operate with a pulse repetition frequency (PRF) under the Nyquist rate, meaning that the azimuth spectrum of each channel will be aliased. This introduces so-called azimuth ambiguities in the resulting SAR image if each channel is processed using traditional monostatic SAR focusing. DBF in azimuth overcomes this challenge by introducing a bank of reconstruction filters and then recombining the information of the channels aligned in azimuth to obtain an equivalent dataset that now satisfies the Nyquist sampling condition [1].

DBF airborne SAR is used to demonstrate the feasibilty of these techniques and to better understand the limitations and potential of the system. Nevertheless, an airborne SAR system does not satisfy all the assumed conditions that apply to spaceborne SAR, like motion inconsistencies. The investigation presented in [2] proposes an enhanced azimuth reconstruction algorithm, that accounts for the possible motion inconsistencies in the system based on [1] and [3]. However, the antenna patterns were assumed to be identical among the azimuth channels, which usually does not match the real scenario of an airborne SAR system, like the DBFSAR airborne system of the German Aerospace Center (DLR) [4]. The correction of antenna pattern differences presents a challenge in HRWS SAR systems, as each individual antenna-modulated Doppler spectrum is aliased.

Hardware design level solutions could be explored to overcome amplitude and phase differences in the antenna diagrams. This could, however, be unfeasible due to limited geometric space and typical boundary conditions, such as complex interactions with the aircraft structure. Alternatively, multichannel data-driven reconstruction algorithms, such as [5], [6], [7], could be used to account for differences in the antenna patterns. However, they cannot correct the variations of the antenna diagrams across Doppler frequency, range frequency, and range simultaneously and depend strongly on input data quality. To overcome these limitations, the use of two-step reconstruction filters, like the ones proposed in [3], can be exploited to perform a three-dimensional correction while keeping the algorithm data-independent.

In particular, the amplitude and phase variation over frequency of the antenna pattern within the imaged swath has not been so far investigated in the context of azimuth reconstruction. Range block processing can be used to find a good compromise between range and wavenumber adaptivity by reducing the range-dependent variation in the wavenumber domain within a single range block. In [3], range block processing is used to reduce the effect of uncompensated polychromatic terms that would introduce considerable phase errors and range shifts in the reconstructed data. However, the antenna patterns were assumed to be identical and rectangular, and the range coverage of a single range block was still in the order of kilometers. If the mentioned dependency in the antenna patterns is taken into account, the block size in range might become more relevant in the definition of the reconstruction algorithm.

The work proposed in this paper enhances the reconstruction algorithm presented in [2]. It includes the differences between the antenna patterns in the definition of the reconstruction filters by exploiting the two-step azimuth reconstruction. Moreover, the importance of using small range blocks to minimize the antenna range frequency dependency over range is shown through a real experiment with the DLR's DBFSAR system.

This paper is organized as follows: Section II presents the antenna patterns as a three-dimensional time-variant compo-

The authors are with the Microwaves and Radar Institute, German Aerospace Center (DLR), 82234 Weßling, Germany (e-mail:Juan.NavarroCastillo@dlr.de). Official published version available at: https://ieeexplore.ieee.org/document/10925493

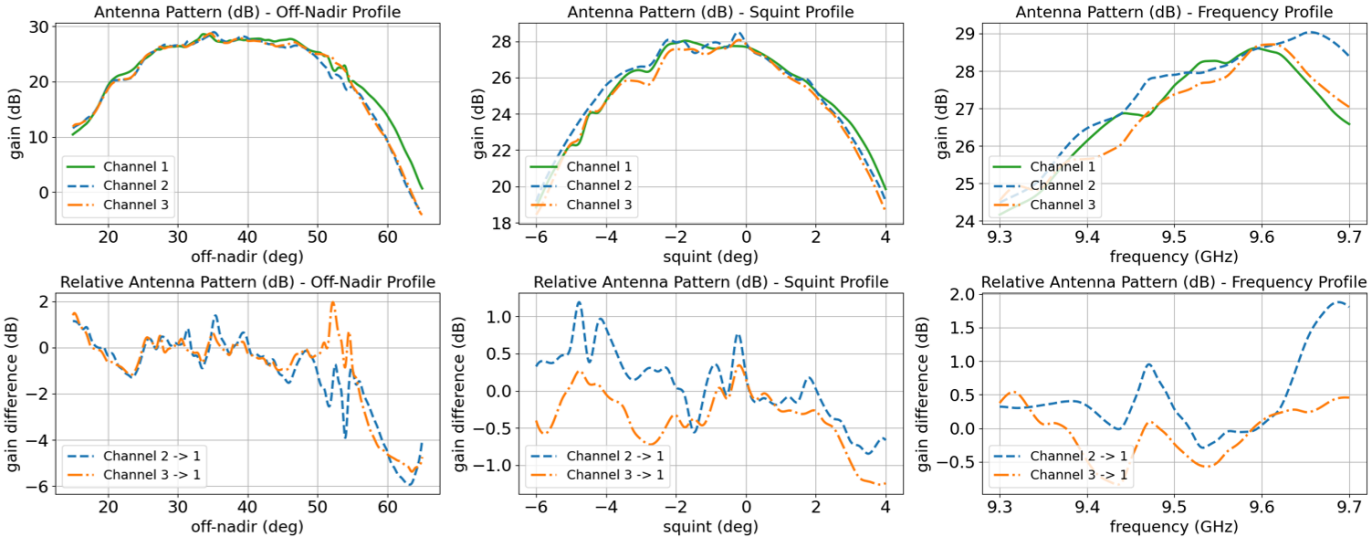

Fig. 1. Real antenna pattern profiles of three channels in the DLR's DBFSAR airborne system (top) and the respective differences between them, relative to channel 1 (bottom). The profiles shown intersect at a frequency of 9.5 GHz, a squint angle of 0 degrees and an off-nadir angle of 40 degrees.

nent and introduces the concept of relative antenna patterns. Section III updates the reconstruction algorithm introduced in [2] by introducing range block processing and the relative antenna patterns in the bistatic impulse response function (IRF). In Section IV the enhanced algorithm is tested with a real multichannel dataset. Finally, Section V summarizes the contributions of this paper.

II. Interchannel Differences Between Antenna Patterns

In DBF SAR systems, each channel has a dedicated receiving antenna. Typically, the receiving radiation patterns in a DBF SAR system are designed to be as close to identical as possible. However, in reality, there exist relative differences between the antenna patterns due to different factors, such as coupling between the individual antenna elements, imperfections during the construction process, the aircraft structure, or the malfunctioning of an antenna sub-module.

In this section, the antenna patterns of the DLR's DBFSAR airborne system are analyzed. This system supports up to six azimuth channels with six independent receiving apertures. The physical separation in azimuth between two contiguous apertures is approximately 0.2 m. For the experiment presented in Section IV, only three channels are used, so that the separation between antennas becomes 0.4 m, such that a quasi-uniform multichannel sample spacing in azimuth can be achieved. This configuration is similar to the one used in the experiments carried out in [2]. More details about the DLR's DBFSAR airborne system and its processing can be found in [4], [8]. In Fig. 1, the major antenna pattern profiles of the selected channels in the DLR's DBFSAR system and their respective relative differences are depicted. The pattern differences will be referred to as relative antenna patterns in this paper and can be expressed as:

$$\Delta\bar{A}_i(f_a, r; f_r) = \frac{\bar{A}_i(f_a, r, f_r)}{\bar{A}_{ref}(f_a, r, f_r)} \tag{1}$$

where $\bar{A}_i(f_a, r, f_r)$ is the effective, range-Doppler projected two-way antenna pattern of the bistatic channel i, and $\bar{A}_{ref}(f_a, r, f_r)$ is the projected reference antenna pattern, both being complex and averaged over the block duration to account for attitude variations during the flight. To reduce the impact of these variations, the use of small azimuth blocks as proposed in [2] is encouraged to prevent large deviations from the actual antenna pattern defined in the reconstruction process. In this study, the reference pattern corresponds to the two-way radiation diagram of one of the bistatic channels. The relative antenna pattern is defined in three dimensions: the Doppler frequency f_a, the slant range r, and the range frequency f_r. The dependency over f_a is directly related to the squint angles which define the azimuth frequency spectrum. Similarly, the variation along r expresses the change of the antenna pattern over the off-nadir angles. Finally, the antenna is designed to work over a certain range of frequencies, which is expressed with the variable f_r. The antenna diagram as defined in (1) is updated in each block based on the attitude angles for the small range of azimuth positions the block covers.

Another important factor is the variation of the frequency dependency of the antenna pattern over range. As an example, Fig. 2 presents the gain and phase of different frequency profiles of $\Delta\bar{A}_2$ using the antenna pattern in channel 1 as reference. The frequency dependency of the relative antenna pattern is not constant over range, meaning that using a single relative antenna pattern for the azimuth reconstruction in the wavenumber domain will introduce considerable residual errors that will deteriorate the azimuth ambiguity-to-signal ratio (AASR). To reduce the magnitude of these residual errors, range block processing can be implemented to minimize the variation of the antenna pattern over range, so that the aforementioned dependency can be considered negligible.

III. Enhanced Motion-Adaptive Reconstruction

The solution proposed in this paper enhances the algorithm presented in [2] by introducing the relative antenna patterns

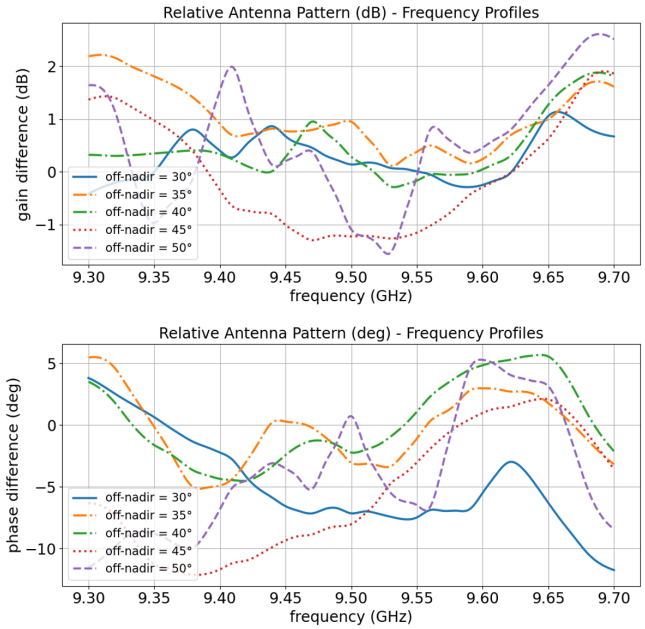

Fig. 2. Gain (top) and phase (bottom) of relative antenna pattern frequency profiles for channel 2 using different off-nadir angles. The frequency axis represents all frequencies within the system bandwidth. The squint angle of the profiles is fixed to 0 degrees.

and range block processing in the definition of the bistatic IRF used to define the reconstruction filters.

Originally, after processing the subsampled input with a beam center relative motion compensation (RelMoCo) algorithm, [2] defines the bistatic IRF of a single azimuth channel i in a DBF SAR system as

$$G_{k,i}(f_{a_k}, r; f_r) = H_{k,ref}(f_{a_k}, r; f_r) \cdot \exp\left[-j \cdot 2\pi \cdot f_{a_k} \cdot \bar{\Delta}t_{k,i}\right] \cdot \bar{E}_{D_{k,i}}(f_{a_k}, r; f_r) \quad (2)$$

where the subscript k indicates the index of the azimuth block. $H_{k,ref}(f_{a_k}, r; f_r)$ is the bistatic IRF of the reference channel (corresponding to channel 1 in this study) for the azimuth block with index k. $\bar{\Delta}t_{k,i}$ is a time delay that depends on the sensor velocity and the distance in azimuth between the phase centers of channel i and the reference channel, averaged over time. $\bar{E}_{D_{k,i}}(f_{a_k}, r; f_r)$ is a Doppler-dependent variable to account for residual irregular motions in DBF airborne SAR and accounts for changes in the topography. The subscript k was added to f_a to indicate the variation of the Doppler centroid (FDC) from block to block due to variable velocity.

The reconstruction filters are then built based on the inversion of the so-called multichannel SAR matrix [2]. This matrix has a shape of $N \times N$, where N denotes the number of azimuth channels. The details about the relation between the bistatic IRF and the multichannel SAR matrix, as well as a further explanation of the elements of the motion-adaptive reconstruction algorithm can be found in [2].

After the reconstruction, the bistatic IRF of the output azimuth block k is equal to $H_{k,ref}(f_{a_k}, r; f_r)$ with a new effective PRF that is N times larger than the original one.

In (2) it is assumed that the antenna patterns are identical and isotropic. However, as discussed before, the antenna patterns are neither isotropic nor identical to each other. Consequently, (2) must be extended by including the antenna pattern of the respective channel. Looking at (1), this pattern can be reformulated as a product of the reference nominal antenna pattern and the relative antenna pattern for that channel. Since the range frequency dependency of the relative antenna patterns varies considerably over range (see Section II), range block processing will be also included in the definition of the bistatic IRF to minimize the impact of this range frequency-dependent variations. After including these new elements in (2), the extended bistatic IRF of an arbitrary channel i after beam center RelMoCo can be expressed as:

$$\hat{G}_{k,l,i}(f_{a_k}, r; f_r) = \bar{W}_{k,l,ref}(f_{a_k}, r; f_r) \cdot \Delta\bar{A}_{k,l,i}(f_{a_k}, r; f_r) \cdot \exp\left[-j \cdot 2\pi \cdot f_{a_k} \cdot \bar{\Delta}t_{k,i}\right] \cdot \bar{E}_{D_{k,l,i}}(f_{a_k}, r; f_r) \quad (3)$$

where

$$\bar{W}_{k,l,ref}(f_{a_k}, r; f_r) = H_{k,l,ref}(f_{a_k}, r; f_r) \cdot \bar{A}_{k,l,ref}(f_{a_k}, r, f_r) \quad (4)$$

The subscript l indicates the index of the range block. This means that suitable correction terms can be defined for a specific azimuth and range block. The channel time delay $\bar{\Delta}t_{k,i}$ is assumed to be constant over range, making it also independent of the range block processing. $\Delta\bar{A}_{k,l,i}(f_{a_k}, r; f_r)$ represents the relative antenna pattern introduced in (1) between the reference channel and the channel i, but defined for a specific azimuth and range processing block. $\bar{W}_{k,l,ref}(f_{a_k}, r; f_r)$ is the reference bistatic IRF that will be obtained after the azimuth reconstruction for the processing block with index k and l. Consequently, the enhanced algorithm corrects additionally the relative differences between the antenna patterns of each azimuth channel. It is assumed that the data provided by the antenna pattern measurements are accurate and representative of the conditions during the flight. After reconstruction, once the range compressed SAR signal is properly sampled, the reference nominal antenna pattern A_{ref} is accounted for in the standard SAR processing.

An overview of the whole processing chain is depicted in Fig. 3. First, the acquired subsampled channels are range compressed. Then, after dividing each channel into K azimuth blocks and applying the beam center RelMoCo, each azimuth block is separated into L range blocks. The range block processing is implemented after the beam center RelMoCo to avoid issues at the block boundaries. Afterwards, the two-step reconstruction is applied. The first bank of reconstruction filters is defined in the wavenumber domain and assumes a constant reference range, usually set in the middle of the block. Consequently, the smaller the range block, the more accurate this assumption will be. Subsequently, the second bank of filters is applied, this time in the range-Doppler domain to account for the rest of the slant ranges. In these filters, the range frequency is constant and equal to the center frequency f_0. This two-step approach serves to suppress the ambiguous power and accounts for the relative Doppler-dependent motion

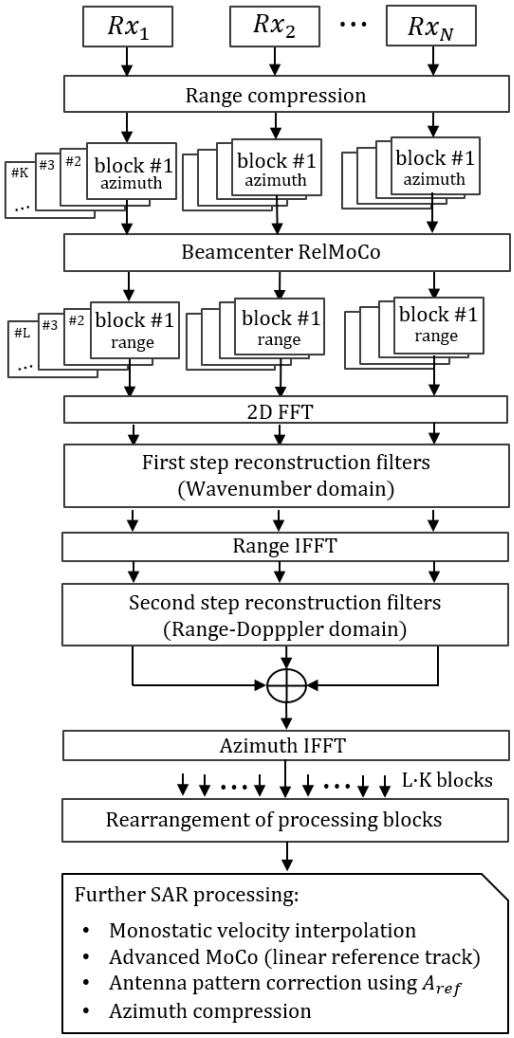

Fig. 3. Block diagram of the proposed reconstruction algorithm for accurate airborne DBF SAR processing with multiple azimuth channels.

components and the relative antenna patterns. After the channels are thus coherently recombined, they are transformed back to the slow-time domain. At this point, the data are properly sampled and with a SAR transfer function equal to (4). Finally, all the reconstructed blocks are rearranged and passed to a SAR processor which applies the standard SAR processing steps that would have been applied to properly sampled range compressed SAR data, including velocity interpolation, motion compensation to a linear track, nominal antenna pattern correction using A_{ref}, and azimuth focusing.

IV. Experimental Results

A multichannel dataset of the DLR's DBFSAR airborne system was used to validate the proposed reconstruction algorithm. The campaign took place in Kaufbeuren, Germany, in 2020. Before the reconstruction, the antenna pointing, the phase center position, system delays and relative channel phase and amplitude offsets have been corrected using the external calibration introduced in [9]. In Table I the relevant parameters for the airborne SAR flight are listed. The 3dB azimuth beamwidth of the two-way antenna corresponds to approximately 600 Hz. To reproduce an undersampled scenario, the data were first processed with a low-pass filter (LPF) to reduce the original azimuth bandwidth to 430 Hz while retaining the full PRF. Then the data were decimated with a factor of 20 by discarding 95% of all range lines to obtain a PRF equal to 150 Hz.

TABLE I
Parameters DBFSAR Experiment

Parameter	Value
Carrier frequency	9.50 GHz
Processed squint angle	-2.83º
Original PRF	3004.80 Hz
Average sensor height	3050 m
Mean velocity	90.11 m/s
Number of receivers	3
Chirp bandwidth	400 MHz

In this section, the multichannel subsampled data are processed using three different reconstruction configurations. The resulting focused SAR images are depicted in Fig. 4. In scenario (a), the multichannel subsampled data are processed with the algorithm proposed in [2], without including any relative antenna pattern or range block processing. Then, in scenario (b), the relative antenna patterns are included in the bistatic IRF, using a range block size close to 2 km. Finally, the scenario (c) also includes the relative antenna patterns but the range block size is reduced to around 20 m. The appropriate range block size will strongly depend on the variation in elevation of the antenna pattern over frequency. If it does not experience rapid variations over range, the block size can be larger to save computational effort. For our experiment, we find the range block size of 64 samples (close to 20 m) to be optimum to compensate for the variations shown in Fig. 2.

For each scenario in Fig. 4, three point targets at different ranges are highlighted. The red Region of Interest (ROI) corresponds to the near range, the green ROI to the middle range and the blue ROI to the far range. The performance of the algorithms is evaluated in each of these ROIs using the AASR. The results are shown in Table II. In this table, there is a fourth scenario that represents a SAR image obtained from the original oversampled raw data.

In all cases, the azimuth resolution achieved was close to the nominal value of 23 cm. In scenario (a), the targets are properly focused but strong azimuth ambiguities are still visible in the three ROIs. In scenario (b), the reference range was set to be exactly at the range of the target in the green ROI. For this reason, the azimuth ambiguities were properly suppressed for this target, but not for the targets in the other two ROIs. In scenario (c), each target was reconstructed in a different range block. In this case, the azimuth ambiguities were correctly removed in all three ROIs. Looking at Table II, it can be observed that the AASR in scenario (c) differs from the reference by less than 1 dB, confirming the very good performance of the proposed approach.

V. Conclusions

This paper presents an enhancement of the motion-adaptive reconstruction algorithm that addresses the challenge of rel-

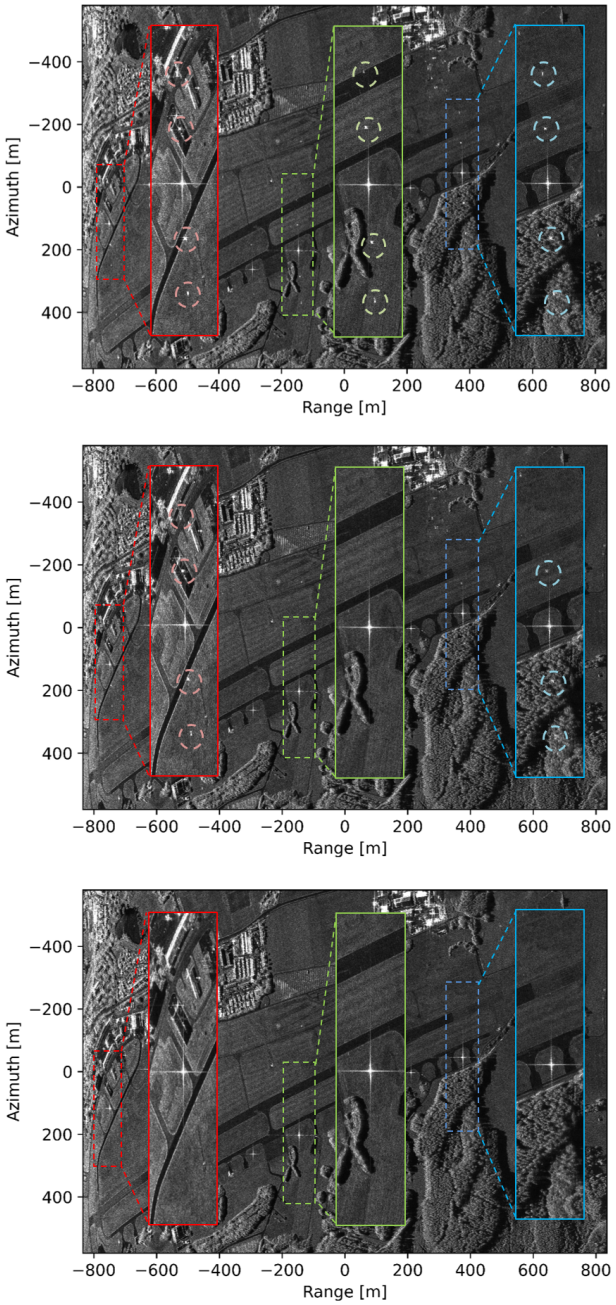

Fig. 4. Focused SAR images for different reconstructions: Neither accounting for the relative antenna patterns nor using range block processing (top). Including the relative antenna patterns in the reconstruction with a range block size of 2 km (middle). Including the relative antenna patterns and using a range block size of 20 m (bottom).

ative differences between antenna patterns across azimuth channels.

The findings underline the efficacy of employing a two-step azimuth reconstruction methodology paired with small block processing. This combination increases the accuracy by adaptively correcting variations in attitude angles during flight and accounting for differences in antenna diagrams across squint, off-nadir, and range frequency dimensions.

The use of this method may extend beyond airborne DBF SAR applications, presenting potential benefits for space-borne HRWS SAR systems facing similar challenges, such as frequency- or propagation direction-dependent differences between antenna diagrams, or across-track baselines. However, this algorithm relies on assumptions that may not hold when azimuth baselines are large, as in distributed multichannel SAR systems [3], [10], [11]. Further research is needed to assess the applicability of these solutions for distributed SAR configurations.

TABLE II
COMPARISON OF AASR FOR THE CONFIGURATIONS SHOWN IN FIG. 4

	Scenario (a)	**Scenario (b)**	**Scenario (c)**	**Reference**
AASR (red ROI)	-22.48 dB	-28.05 dB	-34.44 dB	-35.22 dB
AASR (green ROI)	-27.64 dB	-33.17 dB	-33.20 dB	-33.40 dB
AASR (blue ROI)	-25.34 dB	-27.81 dB	-31.19 dB	-32.06 dB

REFERENCES

[1] G. Krieger, N. Gebert, and A. Moreira, "Unambiguous SAR Signal Reconstruction from Nonuniform Displaced Phase Center Sampling," *IEEE Geoscience and Remote Sensing Letters*, vol. 1, no. 4, pp. 260–264, Oct. 2004.

[2] J. P. N. Castillo, R. Scheiber, M. Jäger, and A. Moreira, "Sub-Aperture Motion-Adaptive Reconstruction Techniques for Digital Beamforming Airborne SAR," *IEEE Transactions on Geoscience and Remote Sensing*, pp. 1–1, 2024.

[3] N. Sakar, M. Rodriguez-Cassola, P. Prats-Iraola, and A. Moreira, "Azimuth Reconstruction Algorithm for Multistatic SAR Formations with Large Along-Track Baselines," *IEEE Transactions on Geoscience and Remote Sensing*, vol. 58, no. 3, pp. 1931–1940, Mar. 2020.

[4] A. Reigber *et al.*, "The High-Resolution Digital-Beamforming Airborne SAR System DBFSAR," *Remote Sensing*, vol. 12, no. 11, p. 1710, May 2020.

[5] Y. Cai *et al.*, "An Efficient Phase Error Calibration Method for Azimuth Multichannel SAR Based on Least Spectrum Difference," *IEEE Transactions on Geoscience and Remote Sensing*, vol. 62, pp. 1–13, 2024.

[6] I. Sikaneta, C. H. Gierull, and D. Cerutti-Maori, "Optimum Signal Processing for Multichannel SAR: With Application to High-Resolution Wide-Swath Imaging," *IEEE Transactions on Geoscience and Remote Sensing*, vol. 52, no. 10, pp. 6095–6109, Oct. 2014.

[7] D. Cerutti-Maori, I. Sikaneta, J. Klare, and C. H. Gierull, "MIMO SAR Processing for Multichannel High-Resolution Wide-Swath Radars," *IEEE Transactions on Geoscience and Remote Sensing*, vol. 52, no. 8, pp. 5034–5055, Aug. 2014.

[8] A. Reigber *et al.*, "Very-High-Resolution Airborne Synthetic Aperture Radar Imaging: Signal Processing and Applications," *Proceedings of the IEEE*, vol. 101, no. 3, pp. 759–783, Mar. 2013.

[9] M. Jäger, R. Scheiber, and A. Reigber, "Robust, Model-Based External Calibration of Multi-Channel Airborne SAR Sensors Using Range Compressed Raw Data," *Remote Sensing*, vol. 11, no. 22, p. 2674, Nov. 2019.

[10] N. Sakar, M. Rodriguez-Cassola, P. Prats-Iraola, and A. Moreira, "Sampling Analysis and Processing Approach for Distributed SAR Constellations with Along-Track Baselines," *IEEE Transactions on Geoscience and Remote Sensing*, vol. 60, pp. 1–12, 2022.

[11] Y. Zhang, P. Lu, and R. Wang, "New Insights Into Alternating Transmitting Mode (ATM) for Bistatic Multichannel SAR," *IEEE Transactions on Geoscience and Remote Sensing*, vol. 62, pp. 1–16, 2024.